Evaluating corrosion and wear resistance of Ni-Fe(Si-Ti)C nanocomposite coating

M. Karimi[a], M.H. Enayati[a], F.S. Sayyedan[b,*]

[a] Department of Materials Engineering, Isfahan University of Technology, Isfahan 8415683111, Iran

[b] Department of Materials Science and Engineering, Faculty of Engineering, Ferdowsi University of Mashhad, Mashhad 917751111, Iran

Abstract

The aim of this study was to optimize the values of current density and carbide concentration in electrodeposition process of Ni-Fe(Si-Ti)C nanocomposite coating on the AISI 304 stainless steel. The optimal current density in each electrolyte was determined using scanning electron microscope (SEM) images and energy-dispersive spectroscopy (EDS) analysis. Corrosion behavior and wear resistance of the optimized coatings were examined by TOEFL polarization test in 3.5 wt.% NaCl solution and ball-on-disk apparatus, respectively. The values of 30 mA/cm^2 and 10 mA/cm^2 were obtained to be the optimal current densities for electrolytes containing 6 g/L and 12-18 g/L double carbide, respectively. Electrochemical measurements declared that the corrosion rate decreased from 0.0829×10^{-5} mA/cm^2 to 0.0208×10^{-5} mA/cm^2 with increasing the concentration of carbide in the electrolyte from 6 g/L to 18 g/L. Moreover, the friction coefficient of the substrate was found to be significantly greater than that of the coated samples.

Keywords: Electrodeposition, SiC, TiC, Corrosion resistance, Wear resistance.

*Corresponding author. Tel.: +98 (51) 3880-5106; Fax: +98 (51) 3880-7182

E-mail address: sayyedan@um.ac.ir (F.S. Sayyedan)

[DOI: 10.22068/ijmse.3922]

1. Introduction

Appropriate surface modification can either avoid or delay the damage of engineering parts. The process of choosing the best way for creating distinctive surface features is complicated as it requires adjusting a range of characteristics and qualities. Furthermore, selecting an appropriate procedure generally needs economic and environmental considerations [1].

Many surface coating techniques have been introduced to improve surface quality in which electrodeposition would be considered as a simple and cost-effective process producing a homogenous and dense coating with good adhesion to the substrate material, generally metals/alloys. Several benefits, including homogeneity of particles' dispersion, low cost, faster deposition rates, applicability for various shaped substrates, continuity of process, and flexibility in deposition conditions, have made the electrodeposition process a major approach to produce composite coatings [1-5].

Nickel (Ni) and related alloys have gained a lot of attention as a coating material because of their advantages, such as superior corrosion and wear resistance. The electrodeposition of Ni-based coatings accounts for around 12% of global Ni usage [6]. In addition to the pure Ni coating, electrodeposition procedure can create Ni-based composite coatings. Carbides (SiC, TiC, and B_4C), nitrides (AlN, TiN, $Si_3 N_4$, and BN), oxides (Al_2O_3 and GO), Borides (ZrB_2 ,TiB_2, and CrB_2), solid lubricants (graphite, BaF_2, and MoS_2), nanorods, nanotubes, and nanowires are some particles that can be employed as the secondary phase in composite

[DOI: 10.22068/ijmse.3922]

coatings [7]. Ni-based coatings can be used in various applications such as aerospace, automotive, marine, medical, electronics, instrumentation, machine tool, and lock industries [3,8].

The Ni-Fe coating is designed to reduce manufacturing costs while simultaneously providing soft magnetic characteristics, strong electrical conductivity, adequate corrosion resistance, and unique optical qualities [9]. Lee et al [10] created nanocrystalline Ni-Fe coating and found that the electrolyte temperature had a considerable impact on the phase structure. To enhance the magnetic and electrochemical properties of Ni-Fe coatings, Pavithra et al [11] created nanocrystalline Ni-Fe alloys. However, according to earlier literature [12], Ni-Fe alloys were not recommended for the manufacturing of MEMS (microelectromechanical systems) due to their poor mechanical properties. The inclusion of second reinforcing phase in a composite coating has an impact on the coating's corrosion behavior and mechanical characteristics. Co-deposition of ceramic particles into the Ni-Fe matrix such as SiC [13], TiC [14],TiO_2 [15], and Al_2O_3 [16] has been reported in many attempts.

TiC is one of the hardest carbides and could be a suitable candidate as a composite reinforcement because of its pronounced properties, namely high melting temperature (3420 K), high hardness (3200 kg/mm^2), high bending strength, low density (4.95 g/cm^2), high mechanical stiffness, high modulus, high electrical conductivity, thermal stability, and superior corrosion and erosion resistance [17]. TiC-reinforced Ni-matrix composites have been continuously improving since

[DOI: 10.22068/ijmse.3922]

the 1960s due to their remarkable mechanical and physical performance even at high temperatures for refractory, abrasive, and structural applications[18].

Further, researchers have explored Ni–SiC composite coatings extensively, owing to their high hardness and Young's modulus, superior wear resistance, high-temperature oxidation resistance, and low cost of SiC particles [19-22]. The co-deposition mechanism of micro and nano-SiC particles incorporated in nickel matrix has been described by Gyftou et al [23]. The mechanical properties of Ni–SiC nano-composites have been studied by Zimmerman et al [19]. They have been utilized to protect the insides of cylinders, combustion engines, and casting molds against friction [20].

Simultaneous application of TiC and SiC as reinforcement material in the Ni-Fe composite coatings can be beneficial with respect to the mechanical characteristics of the coating.

While the effects of SiC and TiC reinforcements on the characteristics of Ni-matrix composites have been studied independently, there are no report focusing on the effects of TiC and SiC reinforcements on the properties of Ni-Fe nanocomposite coatings. So, the aim of this research was to investigate the microstructure, microhardness, wear, and corrosion resistance of Ni-Fe(Ti,Si)C nanocomposite coatings prepared by a co-electrodeposition method.

2. Materials and methods

[DOI: 10.22068/ijmse.3922]

Ni-Fe(Ti,Si)C nanocomposite were electrodeposited from watt's nickel electrolyte containing Fe_2SO_4 (as iron source), SDS (for better dispersion), and suspended TiC and SiC nanoparticles with average diameter of 40-60 nm. The mass ratio of the TiC:SiC was adjusted constant at 6:4. In order to create more stable suspension of TiC and SiC powders, the synthesized bath was treated by ultrasound for 30 min and mechanically stirred for 24 h before the use. The mechanical stirring was also maintained during the electrodeposition process.

The composition of electrodeposition bath and process parameters are summarized in Table 1. AISI 304 stainless steel was used as cathode with a surface area of 2.5 cm^2. Table 2 presents the chemical composition of the substrate. An electrode of nickel ($2\times1\times10$ cm^3) was used as anode. The distance between electrodes was adjusted at 2 cm. The specimens were cold mounted and mechanically polished down to 1200 grit size using abrasive SiC papers. In order to achieve surface activation, the substrates were chemically cleaned by ethanol for 10 min and then etched in 18 vol.% HCl for 50 s. It is noteworthy that combination of anodic and cathodic treatments may be necessary to reach high degree of adhesion, typically in stainless steel and nickel-based alloys. Accordingly, anodic treatment in 70 vol. % H_2SO_4 at 107 mA/cm^2 for 3 min and cathodic treatment in the strike solution (240 g/L $NiCl_2$, 120 ml/L HCl) at 108 mA/cm^2 for 2 min was conducted. The specimens were rinsed in distilled water and immediately placed in the electrodeposition bath. The electrodeposition process was performed in 6, 12, and 18 g/L carbide concentration for different

[DOI: 10.22068/ijmse.3922]

current densities to investigate the effect of carbide content and current density on the microstructure, wear, and corrosion behavior of the coatings. Samples' codes are listed in table 3.

Table 1. Electrodeposition bath composition and process parameters

Bath composition and technology	Concentration and working condition
$NiSO_4 \cdot 6H_2O$ (nickel sulfate hexahydrate)	250 g/L
$NiCl_2 \cdot 6H_2O$ (nickel chloride hexahydrate)	45 g/L
H_3BO_3 (boric acid)	40 g/L
Fe_2SO_4 (Iron III sulfate)	10 g/L
Dodecyl sodium sulfate	1 g/L
Carbide's particle	6,12,18 g/L
Current density	5,10,20,30,40,50 mA/cm^2
pH	3.5-4
Temperature	55 °C
Stirrer rate	500 rpm

Table 2. Chemical composition of AISI 304 stainless steel

Element	C	Si	S	P	Mn	Ni	Cr	Mo	Ti
Wt.%	0.401	0.292	0.030	0.007	2.27	14.7	18.6	0.0404	2.6

[DOI: 10.22068/ijmse.3922]

Table 3. Samples' codes

Samples' codes	Carbide concentration (g/L)	Current density (mA/cm^2)
6-10	6	10
6-20		20
6-30		30
6-40		40
6-50		50
12-5	12	5
12-10		10
12-20		20
12-30		30
18-5	18	5
18-10		10
18-20		20
18-30		30

The surface morphology of the coatings was studied by a scanning electron microscope (SEM, Philips XL30) equipped with an energy-dispersive spectroscopy (EDS) analyzer. To evaluate the crystallite size, an X-ray diffractometer (Philips X'PERT MPD, 40 kV) with Cu Kα radiation (λ=1.5405 Å) was utilized. The crystallite size (d) of coating was calculated by Scherrer Equation (2.1):

$$d = K\lambda/\beta cos\theta \qquad (2.1)$$

[DOI: 10.22068/ijmse.3922]

Where, d is the average crystallite size, K is Scherrer constant of 0.89, λ is wavelength of X-ray radiation used, θ is the angle of diffraction, and β is the diffraction peak semi-height width (radians).

The mass fraction of carbide particles in the coatings could be calculated according to the following relationships[17]:

$$W_{nC} = (M_n/M_{nC}) \times W_n \quad (2.2)$$

Where n is Si and Ti, W_{nC} is the mass fraction (%) in the composite coatings and M is the molar mass (g/mol).

was examined by energy dispersive spectroscopy (EDS) coupledto the SEM.

The Vickers microhardness (HV in kgf mm^{-2}) of Ni-Fe(Ti,Si)C nanocomposite coatings was measured using a Reichert microhardness tester under 50 g load for 10 s and corresponding final values were determined as the average of 5 measurements.

The wear resistance of Ni-Fe(Ti,Si)C nanocomposite coating was examined using a ball-on-disk friction and wear tester under dry sliding conditions at room temperature. The friction coefficient was recorded automatically during the test and worn surface morphologies of Ni-Fe(Ti,Si)C nanocomposite coatings were studied by SEM after testing.

The electrochemical investigation of the coating was performed in 3.5 wt.% NaCl solution using Potentiostat. Potentiodynamic Polarization were used to examine the corrosion behavior. The electrochemical measurements were done using a conventional three-electrode system at room temperature. The electrodeposited

[DOI: 10.22068/ijmse.3922]

coating acted as working electrode, whereas saturated Ag/AgCl electrode and Pt electrode was used as reference and counter electrodes, respectively. The anodic polarization test was carried out by scanning the samples from cathodic region -0.25 V to anodic region +0.25V at scan rate of 100 mV/min, with respect to OCP condition.

3. Results and discussion

Deposition factors such as current density, electrolyte concentration, pH value, deposition time, and bath temperature have significant effects on the physical properties of the coating generated by the electrodeposition technique [24,25]. To test the influence of current density, the pH value, temperature, and electrolyte concentration were all kept constant.

Fig. 1 represents the topographical feature of the composite coating with varying carbide particle loading in the bath. This figure obviously shows a typical nodular surface morphology. It could be observed that the morphology of the coating became smoother and denser as the current density increased [4]. Appropriate current density may substantially raise the electric field force and greatly reduce the thickness of the hydrogen revolution layer, resulting in significant amounts of SiC and TiC nanoparticles being incorporated into the Ni-Fe(Si-Ti)C nanocomposite coating. As a result, carbide nanoparticles precipitated in the active nucleation sites of co-deposition and restricted nucleus development, leading to smooth, uniform, and fine morphology [15,26]. However, by more increasing current density, the surface morphology changed from dense and

[DOI: 10.22068/ijmse.3922]

compact to rough and globular as shown in Fig. 1. The globule size grew up with further increase in current density.

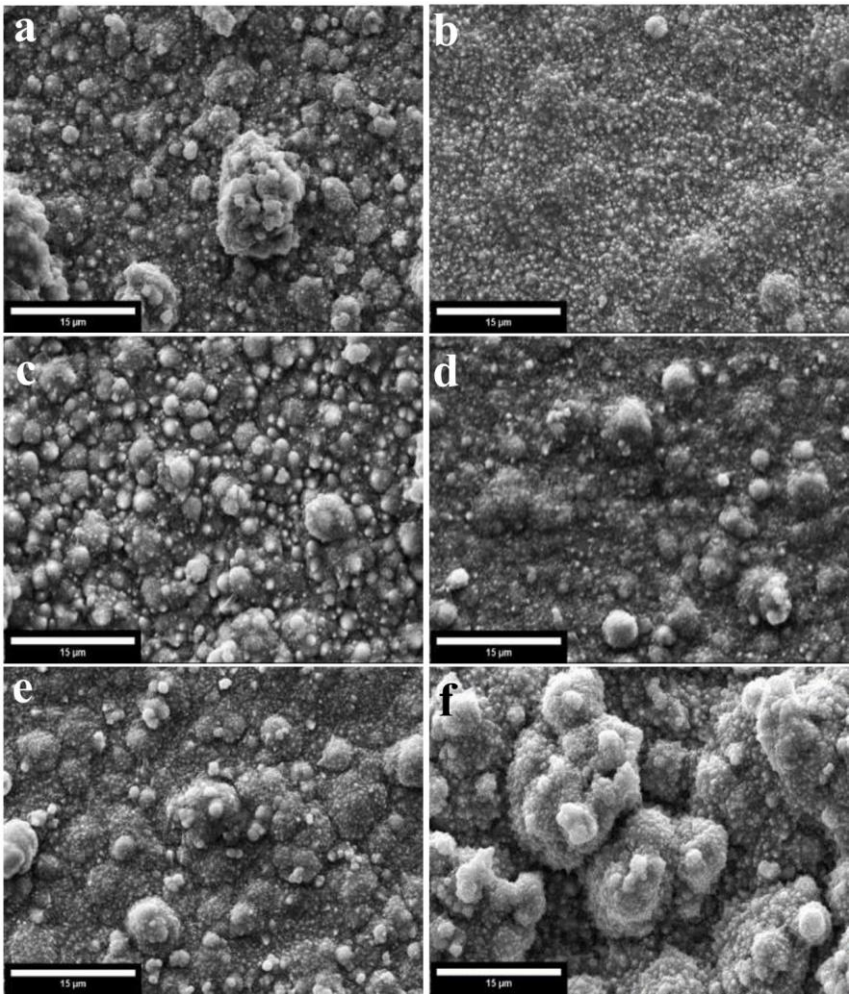

Fig. 1. SEM images of Ni-Fe(SiC-TiC) nanocomposite coating

a) 6-10, b) 6-20, C) 6-30, d) 6-40, e) 6-50

f)12-5, g)12-10, h)12-20, i)12-30

j)18-5, k)18-10, l)18-20, m)18-30.

[DOI: 10.22068/ijmse.3922]

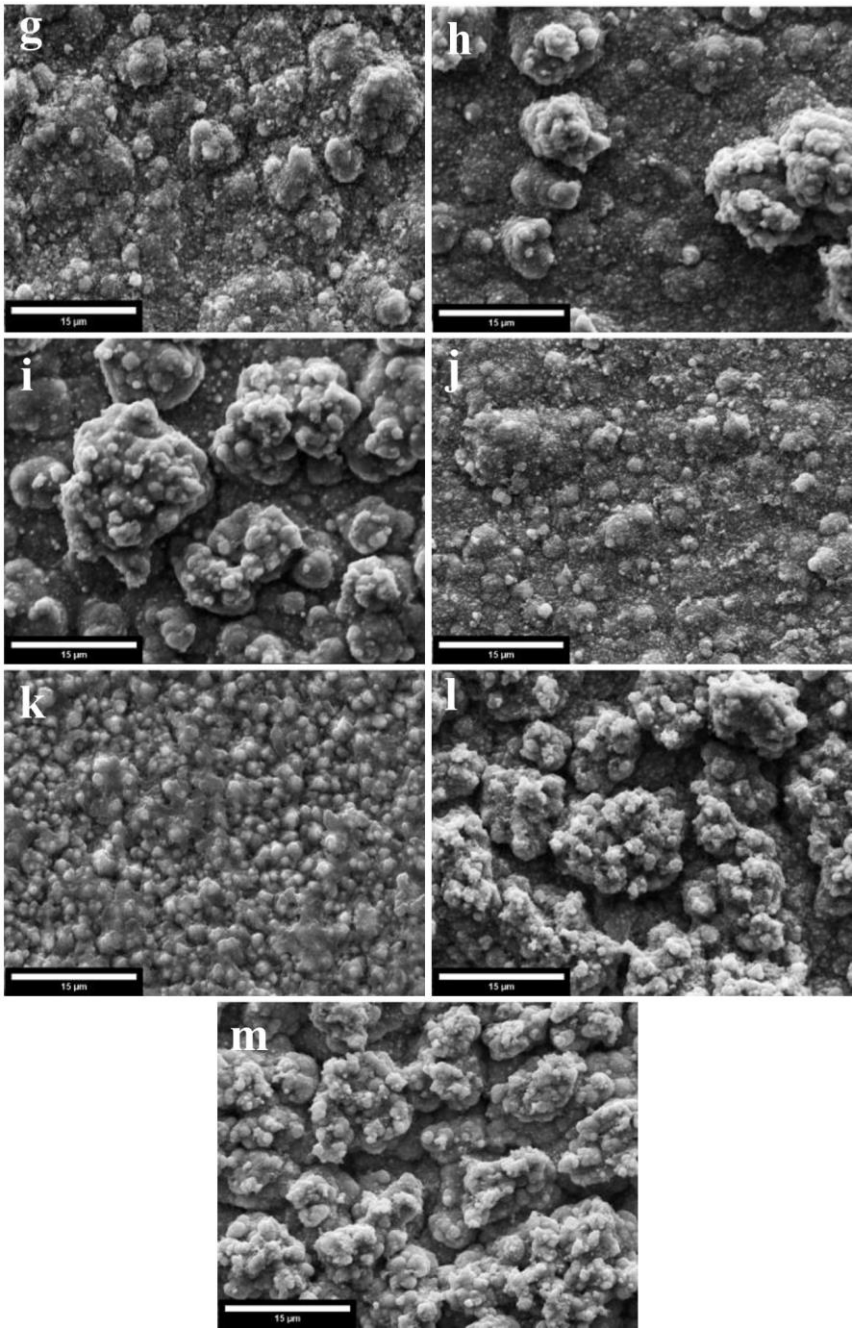

Fig. 1. (Continued)

[DOI: 10.22068/ijmse.3922]

The distribution of Ni, Ti, Si, Fe, and C atoms was analyzed by elemental mapping attached to SEM, as shown in Fig. 2. The homogeneous dispersion of particles in the nanocomposite can be observed.

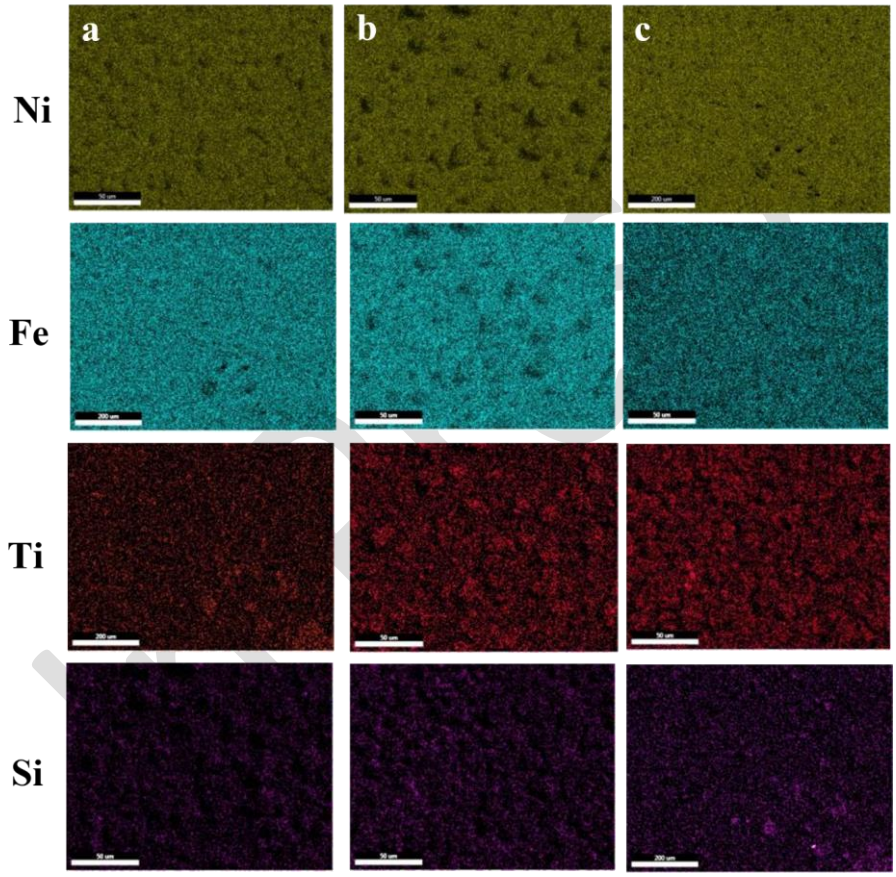

Fig. 2. Elemental mapping analysis of Ni-Fe (SiC-TiC) nanocomposite

a) 6-30, b)12-10, c)18-10.

Fig. 3 shows the cross-sectional SEM micrograph of samples 6-30, 12-10, and 18-10. The coating time was the same in all three samples, so the thickness of the

[DOI: 10.22068/ijmse.3922]

coating was different. As can be seen, the interface of the Ni-Fe(Si-Ti)C coating is smooth, with no porosity and microcrack.

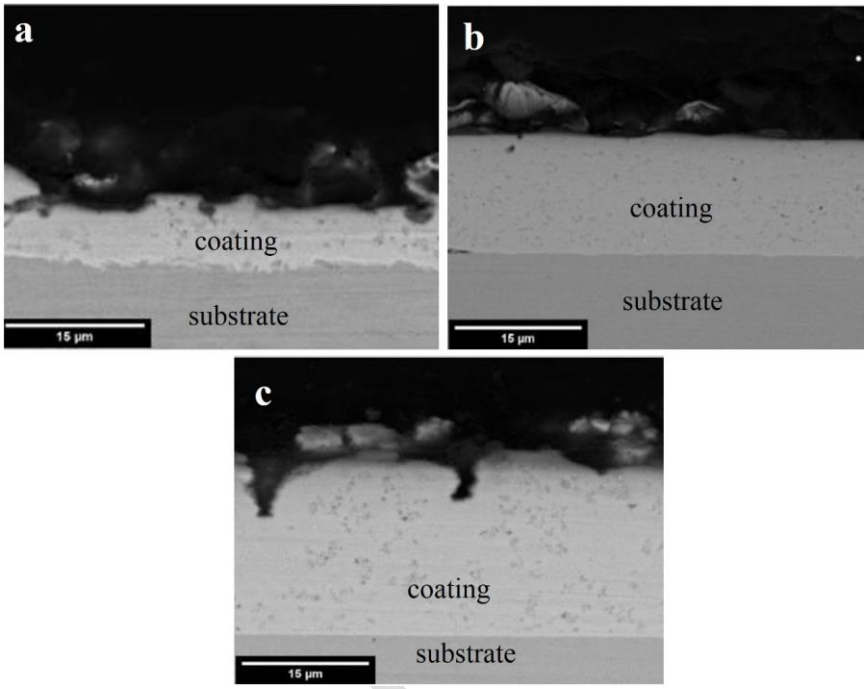

Fig. 3. Cross-sectional SEM micrographs of Ni-Fe (Si-Ti)C composite coatings: a)6-30, b)12-10, c)18-10.

A typical EDS and map of the cross-section for sample 18-10 was developed in order to estimate the chemical characterization of incorporated particles (Fig. 4). It indicated that the Ni-Fe matrix was enriched with Ti and Si elements. Also, the distribution of SiC and TiC particles was different from each other, mainly due to the difference mobility of SiC and TiC particles.

[DOI: 10.22068/ijmse.3922]

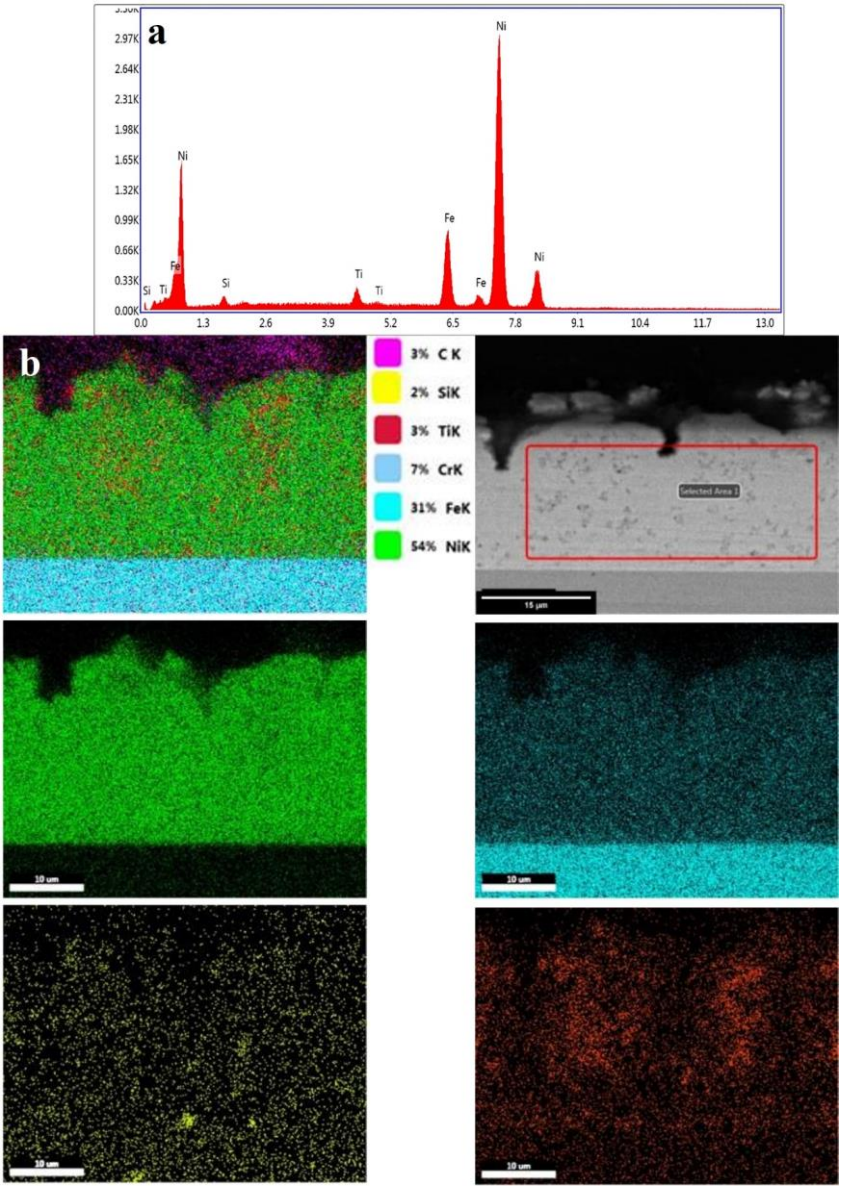

Fig. 4. a) EDS and b) elemental map analysis of Ni-Fe (Si-Ti)C composite coatings in sample18-10.

[DOI: 10.22068/ijmse.3922]

The mass fraction of TiC and SiC in the composite coating with different electrolyte concentrations and current density of 10 mA/cm^2 is presented in Fig. 5. It is obvious that increasing the particle concentration in the electrolyte has increased the incorporation of SiC and TiC particles. As the concentration of carbide particles in the coating rises in a particular range, the number of suspended particles also rises and therefore the number of particles transported to the cathode surface in a certain time enhances. This causes the greater volume fraction of carbide particles are incorporated in the coating. This trend has been confirmed in previous literature [27-30]. The previous literature reported a descending trend for mass fraction of particles after reaching a maximum value, the trend of mass fraction of carbides maintained ascending with increasing carbide content in electrolyte, though (Fig. 5). Lee et al. [31] proposed that the maximum particles incorporated may occur at the particle concentration consistent with steady state equilibrium, where the number of incorporated particles is equal to the number of particles approaching the cathode surface. Accordingly, in this investigation, the carbides content in electrolyte has not yet exceeded the content of carbides in the coating. As a result, with increasing carbides content in electrolyte, the mass fraction in the coating increases.

[DOI: 10.22068/ijmse.3922]

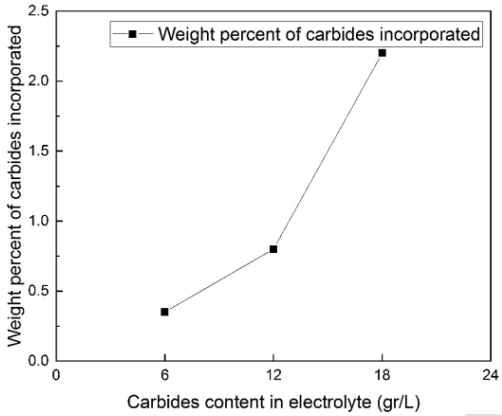

Fig. 5. The effect of carbide content in electrolyte on weight percentage of TiC and SiC carbides incorporated in the Ni-Fe (Si-Ti)C composite coating.

The relationship between the mass fraction of TiC, SiC, and Fe in different current densities over the electrolyte concentration range from 6-18 g/L is shown in Fig. 6. As seen in Fig. 6a, the mass fraction of carbides in coating over current density increases steadily reaching a maximum value and then decreases.

The increasing trend can be explained by the rising tendency for absorbed particles to reach the cathode surface, which is consistent with Guglielmi's model [32]. Guglielmi proposed that in the first stage, the Wonder-Waals force adsorb particles weekly at the cathode, and in the second step, the Coulomb force adsorb particles powerfully at the cathode, causing them to be immersed with deposit metal. According to Faraday's first law, As the current density increases, the Coulomb force increases, and more SiC and TiC nanoparticles are deposited on the cathode.

Formatted: Font color: Text 1

Formatted: Font: (Default) +Headings CS (Times New Roman), Complex Script Font: +Headings CS (Times New Roman)

Formatted: Font: (Default) +Headings CS (Times New Roman), Complex Script Font: +Headings CS (Times New Roman)

Formatted: Font: (Default) +Headings CS (Times New Roman), Complex Script Font: +Headings CS (Times New Roman)

Formatted: Font: (Default) +Headings CS (Times New Roman), Complex Script Font: +Headings CS (Times New Roman)

[DOI: 10.22068/ijmse.3922]

As stated by Beltowska-Lehman et al. [32], the decreasing trend may be attributed to the fact that higher current density leads to faster metal matrix deposition. As a result, fewer carbides particles can be incorporated in the coating. Fig. 6b confirms this observation. It is obvious that the mass fraction of Fe increases with increasing the current density.

According to the surface morphology of the coating presented in Fig. 1 and mass fraction of carbide in Fig. 6a, 30 mA/cm^2, 10 mA/cm^2, and 10 mA/cm^2 were obtained to be the optimal current densities in 6 g/L, 12 g/L, 18 g/L carbide concentrations, respectively, which caused maximum incorporated carbide.

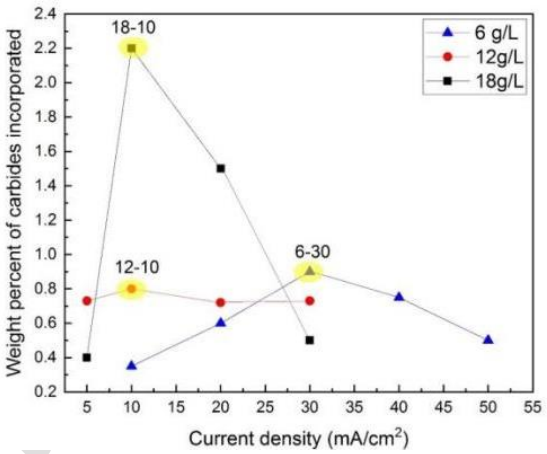

[DOI: 10.22068/ijmse.3922]

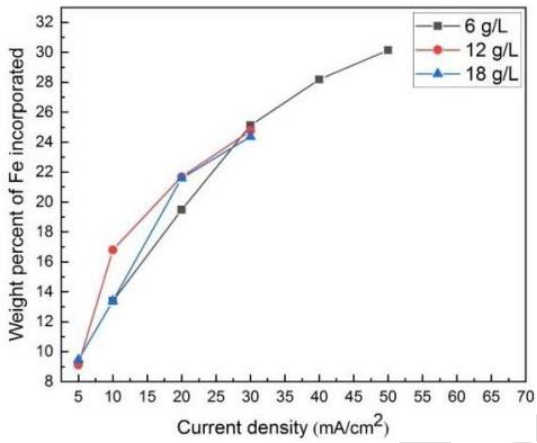

Fig. 6. The effect of current density on the weight percentage of a) TiC and SiC carbides, and b) Fe incorporated in the Ni-Fe (Si-Ti) C composite coating.

The Debye-Scherrer formula was used to estimate the crystallite size of nickel film. The crystallite size in different current densities averaged out for each electrolyte in Table 4. Electrolyte composition and deposition parameters affect the grain size [33]. Increasing the carbide's concentration resulted in decreasing Ni matrix grain size. The regular dispersed Ni embryos and SiC and TiC particles in the Ni matrix restricted the growth of the Ni crystallite, indicating the reduction of crystallite size of the Ni matrix [17]. Carbide nanoparticles adhered to the cathode surface can also operate as nucleation sites during the electrodeposition process, accelerating nickel matrix nucleation. Coating growth is influenced by both nucleation and crystal growth rate [8]. Similar results were reported for Ni-SiC [34], Zn-TiO_2 [35], and Ni–ZrC [36] systems.

[DOI: 10.22068/ijmse.3922]

Table 4. Crystallite size in different current densities averaged out for 6, 12, and 18 g/L carbide concentrations.

Carbide concentration (g/L)	6	12	18
Crystallite size (nm)	318	250	227

Fig. 7. shows the relationship between current density and crystallite size for 18 g/L carbide concentration. Finer crystallite size was achieved with increasing the current density. This phenomenon was expected because increasing the current density causes an increase in nuclear polarization and production rate, which ultimately results in the development of finer crystallites [37,38]. These results were predictable based on the general trends presented by Winand et al [13,39].

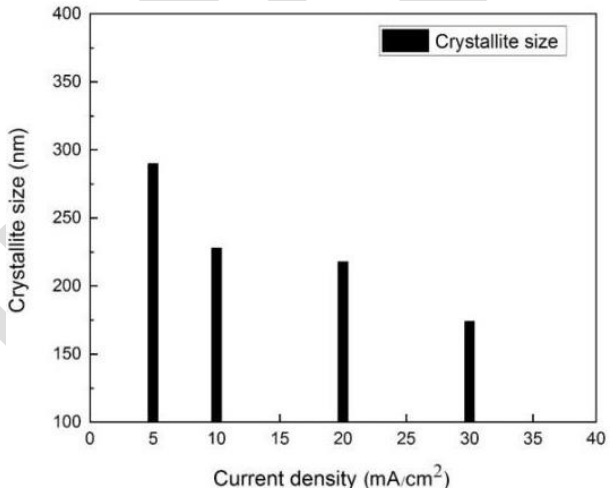

Fig. 7. The effect of current density on the Ni crystallite size of Ni-Fe (Si-Ti)C composite coatings in 18 g/L carbide concentration electrolyte.

[DOI: 10.22068/ijmse.3922]

The microhardness of the composite coating against the carbide content and crystallite size are plotted in Figs. 8 and 9, respectively. Accordingly, it is obvious that the hardness value enhanced with increasing the carbide content in the electrolyte. Dispersion strengthening, the Orawan mechanism, and crystallite size refining are three factors that contribute to improve the coating hardness [17,20,21]. SiC and TiC nanoparticles placed in the nickel matrix could control the growth of nickel crystallites followed by the plastic deformation of the matrix during loading.

More carbide nanoparticle contents lead to the crystallite size refinement and dispersion strengthening effect, and enhance the microhardness of the coating [20,21]. Dislocation bow around carbide nanoparticles, operating as dislocation pinning sites, enhances the flow stress, inversely proportional to the particle dispersion, according to the Orawans hardening theory. Therefore, as the volume percentage of SiC and TiC particulates in the coating increases, particle dispersion decreases, and flow stress increases [8,17,19,38].

Mo et al. [39] found that an increase in the particle content refines the grain size and improves the hardness and wear resistance. Nagayama et al [13] observed that the hardness increased as the SiC content increased in the Fe-Ni/SiC composite film in both heat-treated and un-treated films.

The relationship between the crystallite size and microhardness can be expressed by the Hall-Petch equation, $H=H^{\circ}+Kd^{-1/2}$, where K is a constant, d is crystallite size, H is microhardness, and H° is the intrinsic hardness of the material. This is

[DOI: 10.22068/ijmse.3922]

based on the idea that crystallite boundaries act as barriers to dislocation motion by creating dislocation pile-up at crystallite boundaries, improving microhardness value. Kartal et al [18] concluded that the nickel matrix crystallite size was reduced from 34.48 nm to 26.35 nm by adding TiC reinforcement, followed by an increased coating microhardness.

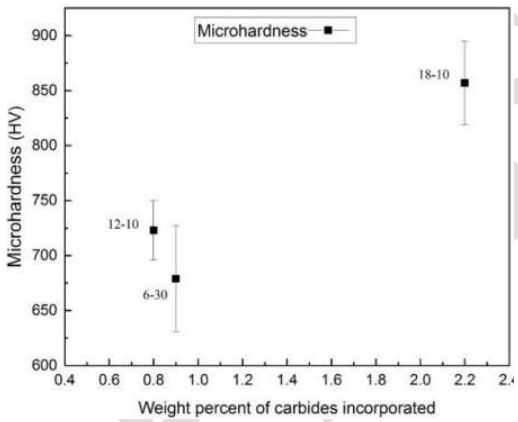

Fig. 8. The effect of weight percentage of carbides incorporated on microhardness of Ni-Fe (Si-Ti)C composite coatings.

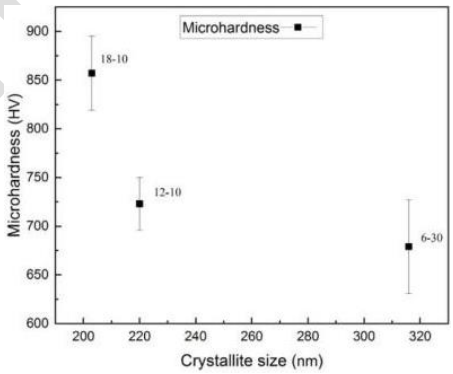

[DOI: 10.22068/ijmse.3922]

Fig. 9. The effect of crystallite size on microhardness of Ni-Fe (Si-Ti)C composite coatings.

The friction coefficient of the substrate, 6-30, 12-10, and 18-10 samples versus sliding distance, obtained from pin on disc test under non-lubricated condition at room temperature is shown in Fig. 10. It was observed that in coated samples, the variations of friction coefficient decreased and became more uniform compared to the bare substrate, and sliding distance increased. TiC and SiC nanoparticle contents and microhardness of coating are the major parameters that determine the friction coefficient of Ni-Fe(Si-Ti)C nanocomposite coating [26]. The presence of harder reinforcing phase into a ductile matrix by a specific volume fraction can reduce the deformation of the matrix in the contact zone due to mitigating wear. Several studies have been conducted in this field. Gül et al [27] used the pulse electrodeposition process to create Ni-SiC composite coatings and the ball-on-disc method to analyze the effect of SiC particle concentration on the coatings' wear resistance. They concluded that the wear rate was significantly reduced with increasing the SiC particle concentration in electrodeposition (from 5 g/L to 20 g/L). This was attributed to the harder coatings and grain refinement and dispersion strengthening by adding carbide particles. Also, Jenczyk et al [40] demonstrated that friction coefficient was increased with an increase in the volume fraction of coated particles in the Ni-SiC composite coatings.

[DOI: 10.22068/ijmse.3922]

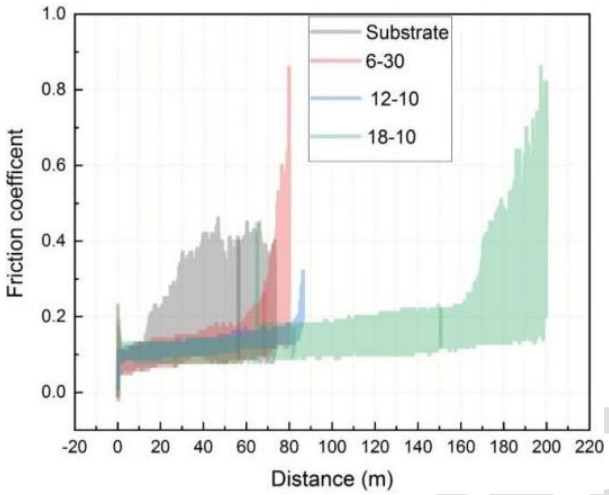

Fig. 10. Friction coefficient of the bare substrate and Ni-Fe (Si-Ti)C composite coatings in optimal samples versus distance.

Figure. 11 displays the surface morphologies of the bare substrate, 6-30, 12-10, and 18-10 samples under same loading. Figure.11 (a and b) shows the substrate morphology with characteristics of adhesion wear. There are obvious plowing and delamination on the surface and large amount of wear and plastic deformation. In Ni-Fe(Si-Ti)C surface, plastic deformation reduced gradually. SiC and TiC nano particles prevent plowing and the effects of wear appear as shallow grooves. Also, as SiC and TiC increasing, wear scars become smoother and narrower with slight scratches. According to these observations, it seems that dominant wear mechanism in the coated samples is abrasive wear. In fact, the reinforcement particles reduce the contact surface with the pin and lead to the reduction of adhesion wear mechanism.

[DOI: 10.22068/ijmse.3922]

In 6-30 morphologies presented in Fig.11 (c and d), the abrasive particle is clear. Separation of materials from the coating surface in abrasive wear mechanism is due to the presence of hard particles on the surface.

The color variation in 12-10 morphologies (Fig. 11e and 11f) demonstrated how the iron separated from 52100 pin and adhered to the counterpart surface. The color difference between nickel and iron has been proven by Hou et al [28]. The EDS analysis of 12-10 specimen (Fig. 11i) confirmed the presence of iron. In addition, the presence of oxygen peaks indicated the oxidation of iron with increasing temperature in the contact zone.

Wear scar in 18-10 morphologies (Fig. 11 g and h) was smooth and only traces of partial wear were observed. The significant amount of reinforcing phase in this coating improved the wear resistance.

[DOI: 10.22068/ijmse.3922]

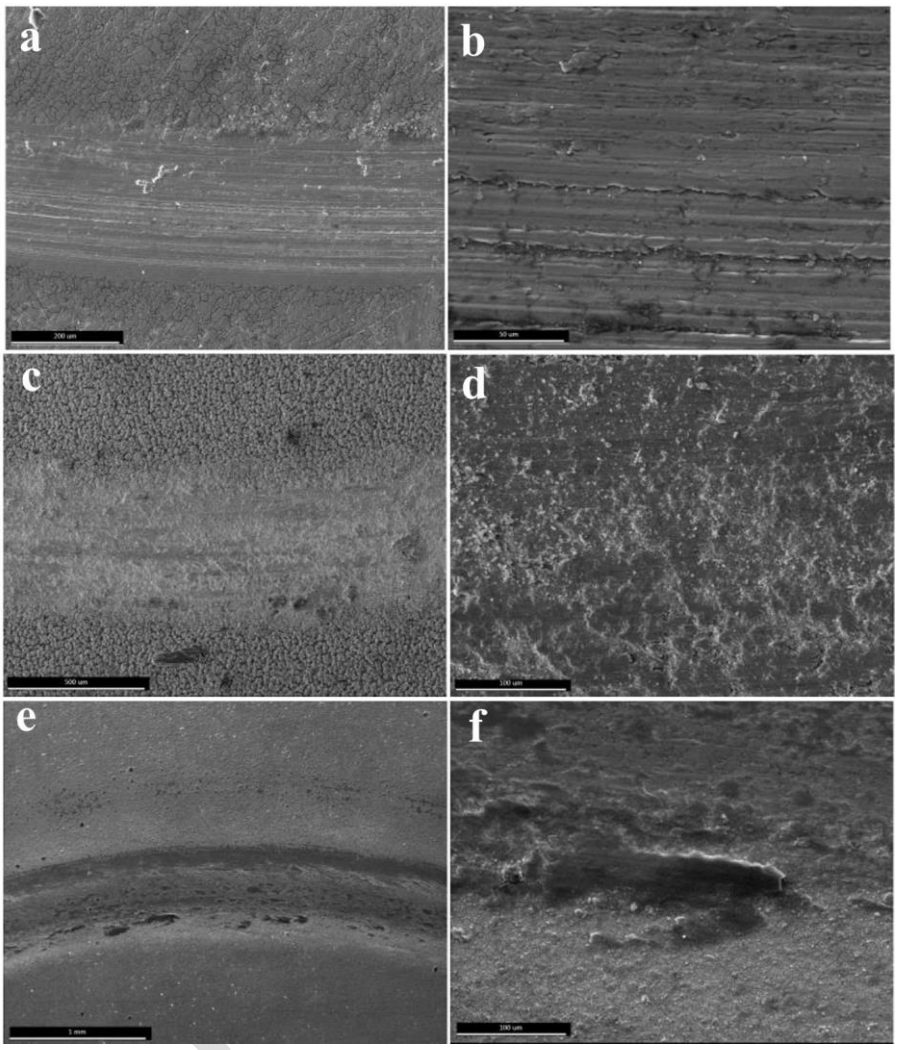

Fig.11. Worn surface morphologies of Ni-Fe (Si-Ti)C coatings

a, b) bare substrate, c, d)6-30, e, f)12-10, g, h)18-10, i)EDS of 12-10.

[DOI: 10.22068/ijmse.3922]

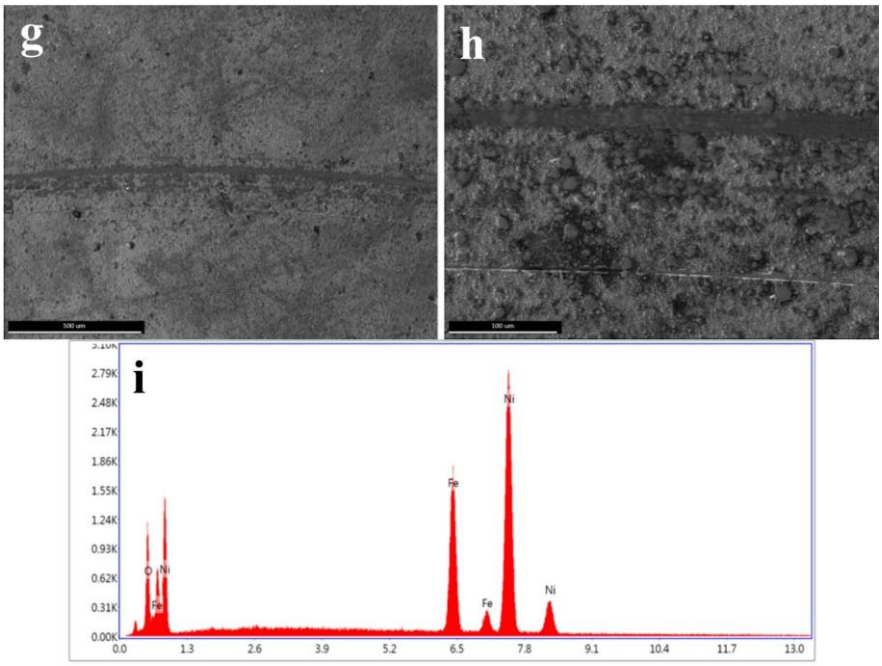

Fig.11. (Continued)

Figure 12 shows the polarization curves of the bare substrate and 6-30, 12-10, 18-10 samples in 3.5 wt.% NaCl solution. The corrosion current density (i_{corr}), corrosion potential (E_{corr}), cathodic and anodic branches slope (βc and βa) values were estimated using Tafel extrapolation method as shown in Table 3. Furthermore, the polarization resistance (Rp) was calculated according to the Stern–Geary equation (equation 1)[42] and reported in Table 3.

Equation 1: $$Rp = \frac{\beta a \times \beta c}{2.303 i corr(\beta a + \beta c)}$$

As can be observed in Fig. 12, all graphs have shown active-passive transition by anodic polarization, but it is obvious that in the coated samples, the corrosion

[DOI: 10.22068/ijmse.3922]

current density decreased and the corrosion potentials shifted to more noble values, which indicates improved corrosion behavior of the bare substrate.

According to Table 3, the polarization resistance of steel substrate was 2.6 $k\Omega.cm^2$ which increased to 180, 251 and 487 $k\Omega.cm^2$ for 6-30, 12-10 and 18-10 coated samples, respectively.

This highly suitable corrosion resistance of the coatings could be due to different reasons. The adsorption of the SiC and TiC nano particles decreases ionic transport such as corrosive ions on the surface, Also, uniform distribution of carbide particles in the coating can fill in crevices, gaps, and micro-holes and create a denser surface [20,41]. Therefore, these particles act as the barrier and limit the penetration path of the corrosive media [22,41].[44].

As can be reported in table 3, the 18-10 coatings with incorporated higher wt. % carbide particles prove to be most resistant in a NaCl solution compared to other samples. As described before, the refinement of the grain size occurred due to the incorporation of more particles, so not only the amount of carbide particles but also the change in microstructure has improved the corrosion rersistance of 18-10 coated sample significantly [45].

[DOI: 10.22068/ijmse.3922]

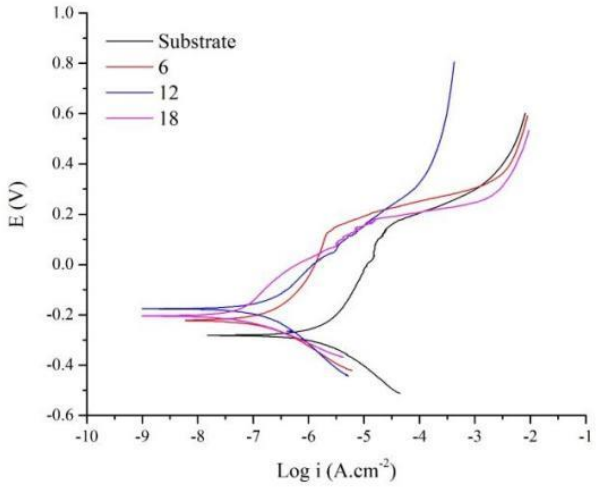

Fig. 12. Polarization curves of the bare substrate and Ni-Fe (Si-Ti)C coatings in 3.5 wt.% NaCl solution.

Table. 5. E_{corr}, i_{corr}, and corrosion rate for Ni-Fe (Si-Ti)C coatings in 3.5 wt.% NaCl

Code	Carbides in electrolyte (g/L)	Carbides incorporating in coating (wt.%)	E_{corr} (mV)	i_{corr} (μA/cm²)	βa (V/dec)	βc (V/dec)	polarization resistance (kΩ.cm²)
Substrate	-	-	-288	1.83	0.35	0.16	2.6
6-30	6	0.9	-235	0.21	0.29	0.13	180
12-10	12	0.8	-182	0.16	0.21	0.17	251
18-10	18	2.2	-208	0.05	0.20	0.07	487

4. Conclusions

In this study, the electrodeposited Ni-Fe(Si-Ti)C nanocomposite coating on the AISI 304 stainless steel surface was developed and optimized under different

[DOI: 10.22068/ijmse.3922]

current densities and concentrations of double carbide. The main results were as follows:

1. The morphology of the coating became smoother and denser with increasing the current density. However, more increasing changed the surface morphology from dense and compact to rough and globular and the globule size grew up.

2. The mass fraction of carbides in the coating over current density increased steadily reaching a maximum value and then decreased. The values of 30 mA/cm^2 for 6 g/L and 10 mA/cm^2 for 12 and 18 g/L electrolytes were chosen as the optimal current densities which caused maximum incorporated carbides.

3. Increasing the current density caused an increase in nuclear polarization and production rate, which ultimately resulted in the development of finer crystallites.

4. The hardness value enhanced from 680 to 855 Vickers by increasing carbide content from 0.9 to 2.2 wt.% in the coating.

5. The variations of friction coefficient decreased and became more uniform and sliding distance increased in coated samples compared to the bare substrate.

6. Coating's corrosion resistance in 3.5 wt.% NaCl solution was improved in comparison to the bare substrate. The corrosion resistance reached from 2.6 kΩ.cm^2 for the bare substrate to 487 kΩ.cm^2 for the sample 18-10.

References

[DOI: 10.22068/ijmse.3922]

1. Torabinejad, V., Aliofkhazraei, M., Assareh, S., Allahyarzadeh, M.H., Rouhaghdam, A.S., "Electrodeposition of Ni-Fe alloys, composites, and nano coatings–A review." *J. Alloys and Compounds.*, 2017, 691, 841-859.
2. Raghavendra, C.R., Basavarajappa, S., Sogalad, I., "Electrodeposition of Ni-nano composite coatings: a review." *J. Inorganic and Nano-Metal Chemistry.*, 2019, 48(12), 583-598.
3. Mahidashti, Z., Aliofkhazraei, M., Lotfi, N., "Review of Nickel-Based Electrodeposited Tribo-Coatings." *J. Transactions of the Indian Institute of Metals.*, 2017, 71(2), 257-295.
4. Khorsand, S., Karbasi, M., Sayyedan, F.S., Eshaghian, M., Razavi, M., "Development of electro-co-deposited Ni–Fe(Ti,W)C nanocomposite coatings." *J. Surface Engineering.*, 2017, 34(6), 433-439.
5. Raja, M., Ramesh Bapu, G.N.K., Maharaja, J., Sekar, R., "Electrodeposition and characterisation of Ni–TiC nanocomposite using Watts bath." *J. Surface Engineering.*, 2014, 30(10), 697-701.
6. Di Bari, G.A., "Electrodeposition of nickel." *J. Modern electroplating.*, 2000, 5, 79-114.
7. Dordsheikh Torkamani, A., Velashjerdi, M., Abbas, A., Bolourchi, M., Maji, P., "Electrodeposition of Nickel matrix composite coatings via various Boride particles: A review." *J. Composites and Compounds.*, 2021, 3(7), 91-98.
8. Wang, P., Cheng, Y.-l., Zhang, Z., "A study on the electrocodeposition processes and properties of Ni–SiC nanocomposite coatings." *J. coatings technology and research.*, 2011, 8(3), 409-417.
9. Kuru, H., Kockar, H., Alper, M., Karaagac, O., "Growth of binary Ni–Fe films: characterisations at low and high potential levels." *J. Magnetism and Magnetic Materials.*, 2015, 377, 59-64.
10. Lee, T.R., Chang, L., Chen, C.-H., "Effect of electrolyte temperature on composition and phase structure of nanocrystalline Fe–Ni alloys prepared by direct current electrodeposition." *J. Surface and Coatings Technology.*, 2012, 207, 523-528.
11. Pavithra, G., Hegde, A.C., "Magnetic property and corrosion resistance of electrodeposited nanocrystalline iron–nickel alloys." *J. Applied Surface Science*., 2012, 258(18), 6884-6890.
12. Yousefi, E., Sharafi, S., Irannejad, A., "The structural, magnetic, and tribological properties of nanocrystalline Fe-Ni permalloy and Fe-Ni-TiO2 composite coatings produced by pulse electro co-deposition." *J. Alloys and Compounds.*, 2018, 753, 308-319.
13. Nagayama, T., Yamamoto, T., Nakamura, T. , Fujiwara, Y., "Properties of electrodeposited invar Fe–Ni alloy/SiC composite film." *J. Surface and Coatings Technology.*, 2017, 322, 70-75.
14. Ganji, M., Yousefnia, H., Seyedraoufi, Z., Shajari, Y., "The corrosion behavior of Ni–Fe and Ni–Fe–TiC nanoparticles deposited using pulse electrodeposition on low-carbon steel." *J. Australian Ceramic Society.*, 2022, 1-13.
15. Ledwig, P., Ratajski, T., Indyka, P., Kalemba-Rec, I., Kopia, A., Kąc, M., Dubiel, B., "Microstructure and Properties of Electrodeposited nc-TiO2/Ni–Fe and Ni–Fe Coatings." *J. Metals and Materials International.*, 2019, 26(6), 812-826.
16. Torabinejad, V., Rouhaghdam, A.S., Aliofkhazraei, M., Allahyarzadeh, M., "Electrodeposition of Ni–Fe and Ni–Fe-(nano Al2O3) multilayer coatings." *J. Alloys and Compounds.*, 2016, 657, 526-536.
17. Ma, M., Sun, W.c., Zhang, Y.g., Liu, X.j., Dong, Y.r., Zi, J.y., Xiao, Y., "Effect of TiC Particles Concentration on Microstructure and Properties of Ni-TiC Composite Coatings." *J. Materials Research.*, 2019, 22(6).
18. Kartal, M., Buyukbayram, I., Alp, A., Akbulut, H., "Production of pulse electrodeposited Ni-TiC nanocomposite coatings." *J. Materials Today: Proceedings.*, 2017, 4(7), 6982-6989.
19. Zimmerman, A., Clark, D., Aust, K., Erb, U., "Pulse electrodeposition of Ni–SiC nanocomposite." *J. Materials letters.*, 2002, 52(1-2), 85-90.
20. Vaezi, M., Sadrnezhaad, S., Nikzad, L., "Electrodeposition of Ni–SiC nano-composite coatings and evaluation of wear and corrosion resistance and electroplating characteristics." *J. Colloids and Surfaces A: Physicochemical and Engineering Aspects.*, 2008, 315(1-3), 176-182.

[DOI: 10.22068/ijmse.3922]

21. Ataee-Esfahani, H., Vaezi, M.R., Nikzad, L., Yazdani, B., Sadrnezhaad, S.K., "Influence of SiC nanoparticles and saccharin on the structure and properties of electrodeposited Ni–Fe/SiC nanocomposite coatings." *J. Alloys and Compounds.*, 2009, 484(1-2), 540-544.
22. Amadeh, A., Rahimi, A., Farshchian, B., Moradi, H., "Corrosion behavior of pulse electrodeposited nanostructure Ni-SiC composite coatings." *J. Nanosci Nanotechnol.*, 2010, 10(8), 5383-5388.
23. Gyftou, P., Pavlatou, E.A., Spyrellis, N., "Effect of pulse electrodeposition parameters on the properties of Ni/nano-SiC composites." *J. Applied Surface Science.*, 2008, 254(18), 5910-5916.
24. Moravej, M., Amira, S., Prima, F., Rahem, A., Fiset, M., Mantovani, D., "Effect of electrodeposition current density on the microstructure and the degradation of electroformed iron for degradable stents." *J. Materials Science and Engineering.*, 2011, 176(20), 1812-1822.
25. Gamboa-Aldeco, M.E., Gale, R.J., A Guide to Problems in Modern Electrochemistry 1: 1: Ionics, Springer Science & Business Media, 2011.
26. Xia, F., Li, Q., Ma, C., Liu, W., Ma, Z., "Preparation and wear properties of Ni/TiN–SiC nanocoatings obtained by pulse current electrodeposition." *J. Ceramics International.*, 2020, 46(6), 7961-7969.
27. Gül, H., Kılıç, F., Uysal, M., Aslan, S., Alp, A., Akbulut, H., "Effect of particle concentration on the structure and tribological properties of submicron particle SiC reinforced Ni metal matrix composite (MMC) coatings produced by electrodeposition." *J. Applied Surface Science.*, 2012, 258(10), 4260-4267.
28. Hou, K., Ger, M., Wang, L., Ke, S., "The wear behaviour of electro-codeposited Ni–SiC composites." *J. Wear.*, 2002, 253(9-10), 994-1003.
29. Spyrellis, N., Pavlatou, E.A., Spanou, S., Zoikis-Karathanasis, A., "Nickel and nickel-phosphorous matrix composite electrocoatings." *J. Transactions of Nonferrous Metals society of china.*, 2009, 19(4), 800-804.
30. Oliver, W.C., Pharr, G.M., "Measurement of hardness and elastic modulus by instrumented indentation: Advances in understanding and refinements to methodology." *J. materials research.*, 2004, 19(1), 3-20.
31. Lee, H.K., Lee, H.Y., Jeon, J.M., "Codeposition of micro-and nano-sized SiC particles in the nickel matrix composite coatings obtained by electroplating." *J. Surface and Coatings Technology.*, 2007, 201(8), 4711-4717.
32. Beltowska-Lehman, E., Indyka, P., Bigos, A., Szczerba, M.J., Kot, M., "Ni–W/ZrO2 nanocomposites obtained by ultrasonic DC electrodeposition." *J. Materials & design.*, 2015, 80, 1-11.
33. Abdel-Karim, R., Reda, Y., Muhammed, M., El-Raghy, S., Shoeib, M., Ahmed, H., "Electrodeposition and Characterization of Nanocrystalline Ni-Fe Alloys." *J. Nanomaterials.*, 2011, 1-8.
34. Gyftou, P., Pavlatou, E., Spyrellis, N., "Effect of pulse electrodeposition parameters on the properties of Ni/nano-SiC composites." *J. Applied surface science.*, 2008, 254(18), 5910-5916.
35. Frade, T., Bouzon, V., Gomes, A., da Silva Pereira, M., "Pulsed-reverse current electrodeposition of Zn and Zn-TiO2 nanocomposite films." *J. Surface and Coatings Technology.*, 2010, 204(21-22), 3592-3598.
36. Zhang, Z., Jiang, C., Cai, F., Fu, P., Ma, N., Ji, V., "Two stages for the evolution of crystallite size and texture of electrodeposited Ni–ZrC composite coating." *J. Surface and Coatings Technology.*, 2015, 261, 122-129.
37. Wei, H.J., Sun, W.C., Hou, G.Q., Zhang, F., Shi, Q., "Application of Artificial Neural Networks to Optimize Processing-Properties of Ni-TiC Composite Coatings." *J. Materials Science Forum.*, 2015, Trans Tech Publ, pp 725-730.

[DOI: 10.22068/ijmse.3922]

38. Sajjadnejad, M., Haghshenas, S.M.S., Badr, P., Setoudeh, N., Hosseinpour, S., "Wear and tribological characterization of nickel matrix electrodeposited composites: A review." *J. Wear.*, 2021, 486-487.
39. Mo, T., Chen, J., Bai, W., Wu, Y., Zhang, P., Zheng, B., "Ni/TiC composite electrodeposition on the surface of Ni-based superalloy." *J. Surface and Coatings Technology.*, 2021, 424.
40. Jenczyk, P., Gawrońska, M., Dera, W., Chrzanowska-Giżyńska, J., Denis, P., Jarząbek, D.M., "Application of SiC particles coated with a protective Ni layer for production of Ni/SiC co-electrodeposited composite coatings with enhanced tribological properties." *J. Ceramics International.*, 2019, 45(17), 23540-23547.
41. Fayyaz, O., Khan, A., Shakoor, R., Hasan, A., Yusuf, M.M., Montemor, M., Rasul, S., Khan, K., Faruque, M., Okonkwo, P.C., "Enhancement of mechanical and corrosion resistance properties of electrodeposited Ni–P–TiC composite coatings." *J. Scientific Reports.*, 2021, 11(1), 1-16 .

Formatted: Font: Not Italic, Complex Script Font: Italic

Formatted: Complex Script Font: Bold

Formatted: Font: Italic, Complex Script Font: Italic

Formatted: Font: Italic, Complex Script Font: Italic

[DOI: 10.22068/ijmse.3922]